Fa-acél hibrid híd: mért és számított eredmények összehasonlítása

Kivonat

Japánban egyre több kutatási program koncentrál japán cédrust alkalmazó mérnöki megoldásokra. E kezdeményezések részeként a szerzők egy olyan kiemelkedő tartósságú, rövid és közepes fesztávolságú fahíd fejlesztésére fókuszálnak, mely japán cédrus rétegelt-ragasztott tartó és acél felhasználásával készül. Korábbi munkáikra támaszkodva, a rétegelt-ragasztott gerenda – ortotróp acél borítás hibrid szerkezet tulajdonságainak vizsgálatával folytatva valósítják meg a kitűzött tervet. E cikkben egy kicsinyített léptékű vizsgálat mérési eredményeit hasonlítják össze végeselem módszerrel illetve a plasztikus kompozit gerendák elmélete alapján számított eredményekkel. A mérési eredmények egy 1:3 léptékű, 5,0 m fesztávolságú, 2,1 m széles hibrid híd modellen végrehajtott tönkremeneteli vizsgálatból származnak. A rétegelt-ragasztott tartó – acél rendszer egy ortotróp acélborításból és két dupla rétegelt-ragasztott gerendából áll, melyek felső élébe egy, alsó élébe kettő acél szalagot ragasztottak vertikálisan epoxi gyantával. A végeselem modell csak a vizsgált hibrid szerkezet egynegyedét tartalmazza a kötések egyszerűsített modellezésével. Minden szerkezeti elemet szilárd elemként modelleztek.

Kulcsszavak: japán cédrus, rétegelt-ragasztott tartó, hibrid híd, végeselem modell

Introduction

Using the widely available Japanese cedar (Cryptomeria japonica) in civil engineering applications has become a priority research theme in Japan, resulting in an increasing number of research projects focusing on this material. As a part of these efforts, the authors have been working on developing a highly durable timber bridge, using a hybrid structural system, comprising Japanese cedar glulam main and floor beams, as well as an orthotropic steel deck. In accomplishing their goal, the authors investigated the structural performance of this hybrid system. The ongoing study focuses on the comparison of the measured results, observed during bending and failure tests, and the calculated results, obtained from two analytical methods: plastic composite beam theory and the finite element method (Kiss et al. 2008, Kiss et al. 2007a). The authors introduced this hybrid structure for short and medium span bridges in their previous works (Kiss et al. 2007b, Kiss et al. 2006a, Kiss et al. 2006b). A comprehensible design method was necessary in order to let clients and bridge designers know about the advantages and possibilities of this type of bridge structure. Earlier, the authors proposed the use of plastic composite beam theory as a simple but reliable way of design for this type of bridge. In order to validate the adaptability of this approach for this hybrid system, experimental verification was necessary. Therefore the authors prepared a reduced scale model of the timber-steel hybrid bridge. In order to promote the use of the Japanese cedar for structural applications, a material widely planted in Japan, in this newly designed structure Japanese cedar glulam replaced Douglas fir, which was initially used for the glulam main beams. As a result of this material replacement, Japanese cedar was used not only for the main beams, but also for the floor beams (instead of steel floor beams used initially).

In addition to the simplified analytical approach (plastic composite beam theory) and testing of the structure, a three-dimensional finite element analysis was necessary. Results from the analytical approach using plastic composite beam theory are presented together with results from the FEM analysis. These are compared to measured results from bending and failure tests. This paper presents results focusing mainly on the deformed shape, as well as deflection and strain distributions of the hybrid structure, using the three available sets of results, i.e. from the tests performed, from the plastic composite beam theory and from the FEM analysis.

Experimental Setup

The timber-steel hybrid bridge model was set up, then equipped with measuring instruments and subjected to bending and failure tests at the

structural testing laboratory of the Institute of Wood Technology, Akita Prefectural University, situated in Noshiro City, Japan. The tested structure comprised an orthotropic steel deck, attached through epoxy glued-in steel ribs to two double glulam main beams made of Japanese cedar. It was a reduced model, shown in Fig. 1, the scale being one-third of the prototype bridge (Kiss et al. 2006b).

The hybrid bridge model had a total length of 5.2 m (span being 5.0 m) and a width of 2067 mm. The steel deck was built up of a deck plate (with thickness td = 4.5 mm), stiffened by eight U-shaped longitudinal ribs and seven double glulam floor beams (60x250 mm each), arranged with an interval of 833 mm. A width variation of each main beam took place from width b = 60 mm to 93.5 mm at near beam-ends, in order to overcome shear forces developing by the reactions on supports. This variation happened over a length of 335 mm, the length of widened beam portion becoming equal to 1015 mm, about $^1/_5$ of the total bridge length (Kiss et al. 2006b). The depth of the main beams was h = 300 mm.

Fig.1 shows the cross section of the widened main beam at the support on the left side and the cross section of the main beam at midspan on the right side. Main beams were reinforced by two sets of vertically inserted, epoxy glued-in steel ribs. The compression reinforcement was a single rib of 3x44 mm, while the tension reinforcement was a double rib of 6x70 mm each. The timber was Japanese cedar of strength grade E75-F240 JAS, while steel was SS400.

For timber, measured modulus of rupture $\sigma_{y,W}$ = 39 MPa, measured modulus of elasticity E_W = 9 GPa, and shear modulus G_W = 601 MPa were applied. For steel, measured yield strength $\sigma_{y,S}$ = 297 MPa, allowable bending stress σ_{ba} = 137 MPa, and modulus of elasticity E_S = 206 GPa were used. The timber-steel bridge was designed using plastic composite beam theory, all steel being converted to an equivalent wood area (Kiss et al. 2006b).

Prior to undergoing the failure test, the hybrid model was subjected to nine bending tests, corresponding to nine loading cases. The difference between these scenarios was the position of the applied truck wheel load (Kiss et al. 2007b). A load-controlled testing machine loaded the simply supported model. Results of one of the bending tests (at load case LC1) and of the failure test (at load case LC2) are presented later in this paper. A total number of 100 strain gauges were installed at four different cross sections along the timber-steel bridge model. At section B-B (midspan) gauges were installed at the bottom of floor beams, to steel side plates and to lower inserted ribs. At sections C-C (350 mm from midspan) and D-D (Fig. 13) gauges were applied along the depth of the main beams, to the upper surface of the orthotropic steel deck and to the bottom of the U-ribs (Kiss et al. 2006a).

Finite Element Analysis

The epoxy glued-in single steel rib on the compression side of each glulam main beam served as a shear connector between the upper and lower structure of the hybrid model, i.e. the steel deck and the glulam

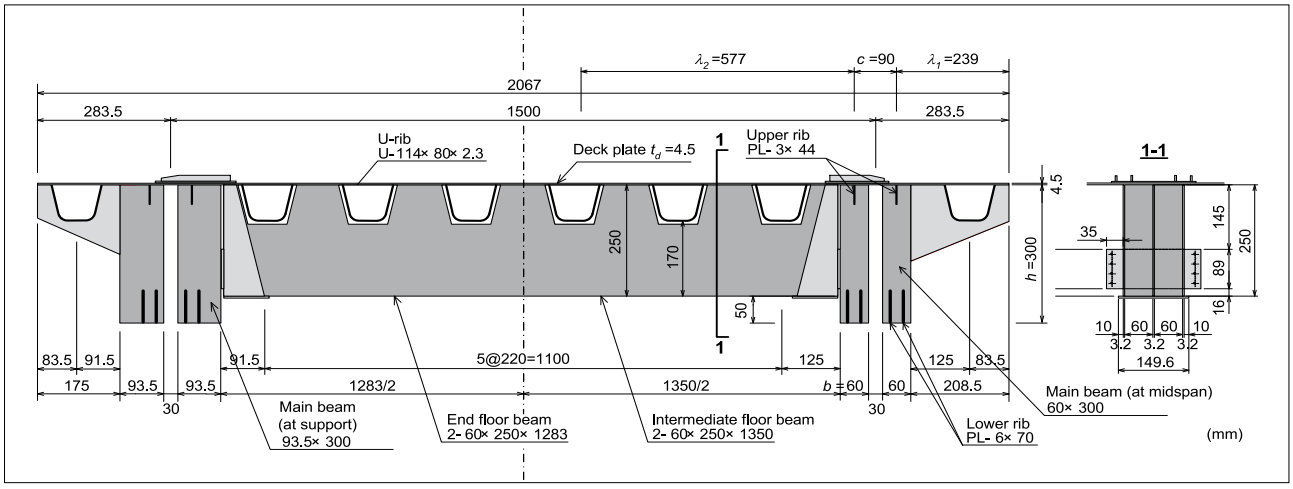

Fig. 1 Hybrid bridge model cross section (left: at support, right: at midspan)

1. ábra A hibrid híd modell keresztmetszete (bal oldalon az alátámasztásnál, jobb oldalon a fesztáv közepén)

main beams. The role of the epoxy glued-in double steel rib on the tension side of each main beam was to compensate the longitudinal axial strength. Thus, a part of the steel deck (determined by the effective widths λ_1 = 239 mm and λ_2 = 577 mm, obtained by applying the Japanese shear lag formula for roadway bridges), the upper and lower ribs and the double glulam main beam formed a composite beam. Therefore, the plastic composite beam theory was applied to calculate the bending and shear stresses (Kiss et al. 2006b). The composite beam was defined as the timber-steel hybrid structure within the width $\lambda_1 + c + \lambda_2$ (see Fig. 1).

Performing a three-dimensional finite element analysis was the next step in understanding the behavior of the proposed timber-steel hybrid bridge. In addition to the already existing experimental and analytical study, finite element calculations were performed by ANSYS Academy Teaching Introductory v11.0, which is a general purpose FEM package. Among other mechanical problems, the ANSYS package can also be used for static non-linear structural analysis. Considering the loading scheme during testing and taking advantage of the geometric symmetry, only half of the tested structure was modeled for the analysis (see Fig. 4 and Fig. 8). Symmetry boundary conditions were applied at midspan and the structure was simply supported.

In order to obtain reliable results in the FEM, accurate modeling of material properties is important. Japanese cedar glulam was of strength grade E75-F240, steel was SS400 (Fig. 2). Timber was modeled as an elasto-plastic orthotropic material with a bilinear stress-strain curve, using a bending moment capacity equal to $\sigma_{y,W}$ = 39 MPa. The following values of Young's modulus, shear modulus and Poisson's ratio were used: E_Z = 9 GPa, $E_X = E_Y$ = 300 MPa, $G_{YZ} = G_{XZ}$ = 601 MPa, G_{XY} = 60 MPa, $\nu_{YZ} = \nu_{XZ}$ = 0.01, ν_{XY} = 0.2, where Z-axis is parallel to grain. Steel was modeled as a perfect elasto-plastic isotropic material, with the values E_S = 206 GPa, ν_S = 0.3, together with a yield strength of $\sigma_{y,S}$ = 297 MPa. The applied truck wheel load was modeled as a pair of uniformly distributed loads. The geometric model was used to create a mesh of 8-node solid elements with different sizes, comprising 21,266 elements and 21,170 nodes in total (Miki et al. 2005, Pousette 2003).

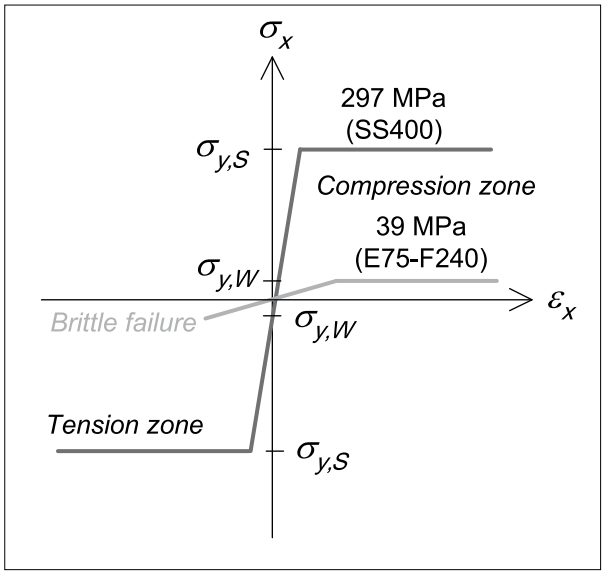

Fig. 2 Material models applied in the analysis
2. ábra Az analízis során alkalmazott anyagmodellek

Results and Discussions

Bending Test (Load Case LC1)

The hybrid model shown in Fig. 3 was subjected to bending in load case LC1, prior to other bending tests (Kiss et al. 2007b), not discussed here, and failure test in load case LC2. A half-structure three-dimensional model (Fig. 4) was created for this load case. Fig. 5 shows the deformed shape of the FEM model at midspan (magnified 10 times for better visibility) at load P = 120 kN. Measured and calculated deflections are shown in Table 1 and compared to each other in Fig. 6. In the test, glulam floor beams and main beams were not connected to each other in order to check the effectiveness of the special structural members (situated on top of the main beams) used for load transfer from floor beams to main beams (Fig. 1). Table 1 shows a disagreement between experimental and analytical data, due to these special structural members not being modeled at this stage of the FEM analysis. Both in the test and in the analysis, floor beams were connected only to the steel deck plate.

Failure Test (Load Case LC2)

The failure test in load case LC2, shown in Fig. 7, took place after the bending tests performed in load case LC1 and other load cases. The corresponding FEM model is shown in Fig. 8. Based on the applied material models, a non-linear static analysis was performed. Fig. 9 shows the hybrid bridge model during testing at plastic load P_P and ultimate load P_U, while Fig. 10 shows the

Fig. 3 Bridge model in load case LC1
3. ábra A hídmodell az LC1 terhelés esetében

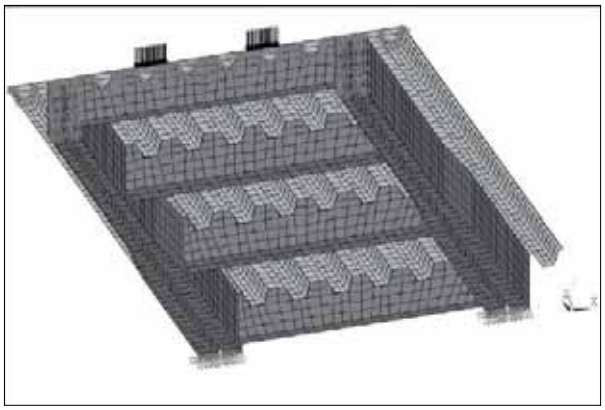

Fig. 4 Finite element model in load case LC1
4. ábra A végeselem modell az LC1 terhelés esetében

Table 1 Deflections for loading scenaio LC1
1. táblázat Alakváltozások az LC1 terhelés esetében

Section	Deflection meter	δ (mm)	
		Test	FEM
B - B	CH2	8,4	7,5
	CH1	8,3	7,5
C - C	CH5	13,8	15,1
	CH4	13,5	15,0
	CH3	13,9	15,1

Fig. 5 Deformed shape at load P = 120 kN (magnified 10 times)
5. ábra Deformálódott alak P=120 kN nagyságú terhelésnél (10-szeres nagyítás)

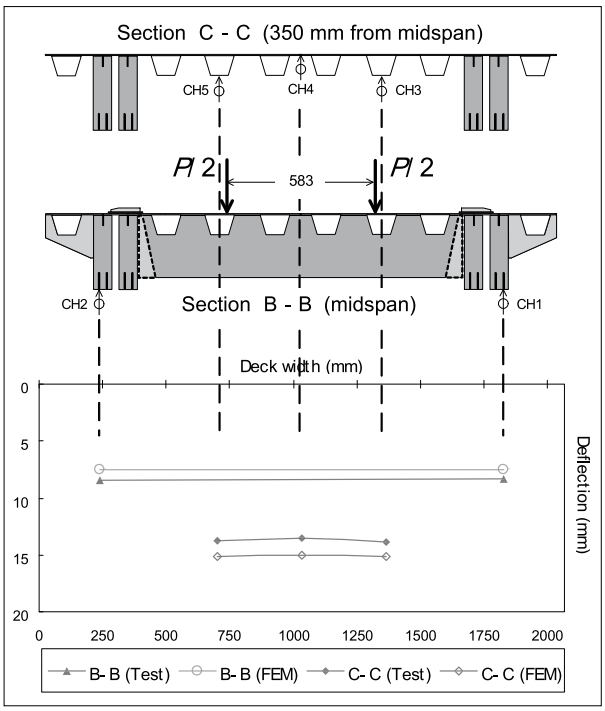

Fig. 6 Deflection distribution at load P = 120 kN
6. ábra A behajlás eloszlása P=120 kN nagyságú terhelésnél

accompanying load-deflection curves, capturing only a portion of the ductile experimental curve (Kiss et al. 2006a).

Calculated P-δ curves determined for deflection meters CH2 and CH1 at midspan by the plastic composite beam theory (PCBT), along with curves resulting from the FEM analysis are included here, the latter being in good agreement with the measured ones. Yield load P_Y, plastic load P_P and ultimate load P_U were determined by the plastic composite beam theory (Kiss et al. 2006b). This theory assumes that at yield load P_Y, the steel of lower rib at deflection meter CH2 reaches its yield strength and starts to yield: in the FEM analysis, this happened at a load larger than the assumed yield load (see Fig.10).

However, at plastic load P_P, the whole lower rib at midspan was in a fully plastic state, as assumed by the PCBT. At ultimate load P_U, the glulam of main beam at deflection meter CH2 did not reach its modulus of rupture as predicted by the PCBT: in the FEM analysis, this happened at the experimental ultimate load $P_{U,exp}$, when is the load where ductile failure of the structure started to begin during testing.

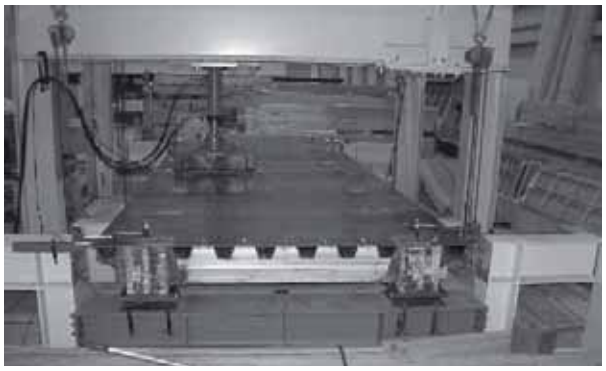

Fig. 7 Bridge model in load case LC2

7. ábra A hídmodell az LC2 terhelés esetében

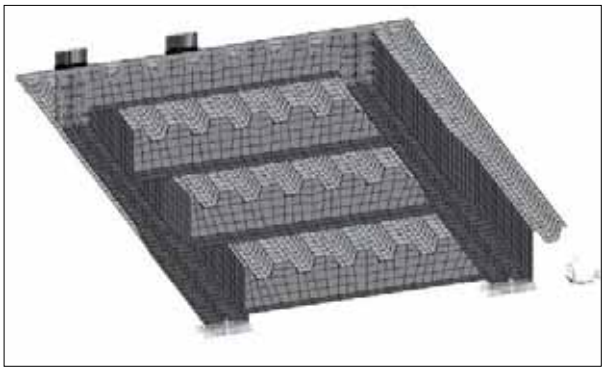

Fig. 8 Finite element model in load case LC2

8. ábra A végeselem modell az LC2 terhelés esetében

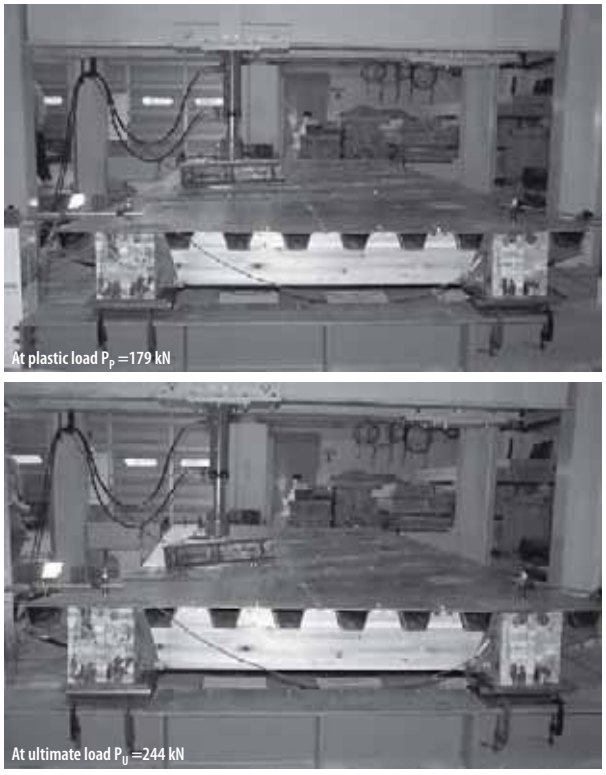

Fig. 9 Bridge model shown during loading

9. ábra A híd modell terhelés közben

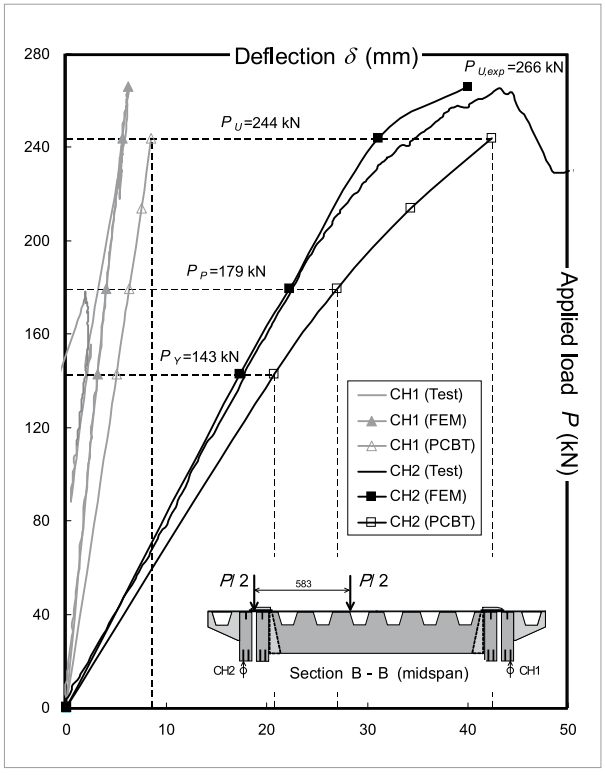

Fig. 10 Comparison of load-deflection curves (detail)

10. ábra A terhelés-alakváltozás görbék összehasonlítása

Failure of the bridge model occurred in a ductile manner, as concluded from the observed failure mechanism during the test. Eight distinct failure positions were detected (Kiss et al. 2006b). Flexural failure started from a knot situated at the tension side of main beam G4, near midspan (Fig. 13). Then failure propagated due to a horizontal crack, close to the first failure position. Glue line represented a major a cause of premature failure, proven by the next failure, i.e. separation of glulam and glue from the lower ribs of main beam G3. The fourth, fifth and sixth positions also exhibited flexural failure. Shear failure occurred at the seventh position (close to the neutral axis) and eighth (final) failure position. Up to the seventh position, the deck plate and U-ribs were in an elastic state. Nevertheless, at the final position, U-ribs were already in a plastic state.

The deformed shape of hybrid structure at midspan (shown in Fig. 11) was obtained from the FEM analysis under each applied truck wheel load P_N (N = Y, P, U), calculated by the plastic composite beam theory. Note that the deformed shapes from the FEM analysis are magnified 10 times to provide better visibility. Fig. 12 shows the deflection distributions at loads P_N (N = Y, P, U). Three sets of deflection are included: first, experimental deflections of main beams G4 and G2, measured at section B-B by deflection meters CH2 and CH1, as well as experimental deflections of U-ribs, measured at section C-C by

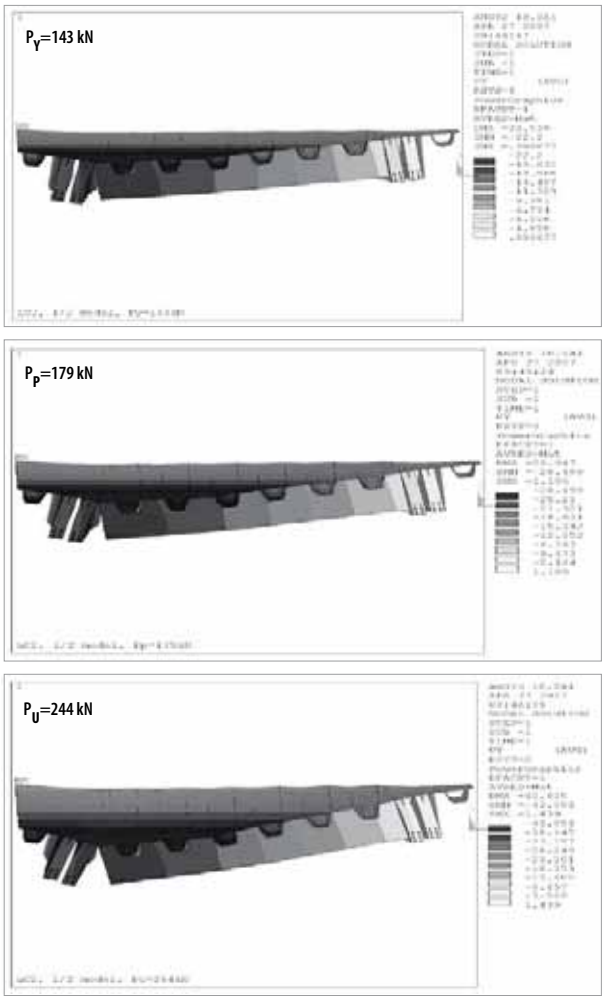

Fig. 11 11 Deformed shape at applied loads P_N (N = Y, P, U) (magnified 10 times)

11. ábra Torzult alakok az alkalmazott P_N terheléseknél (N = Y, P, U, 10-szeres nagyítás)

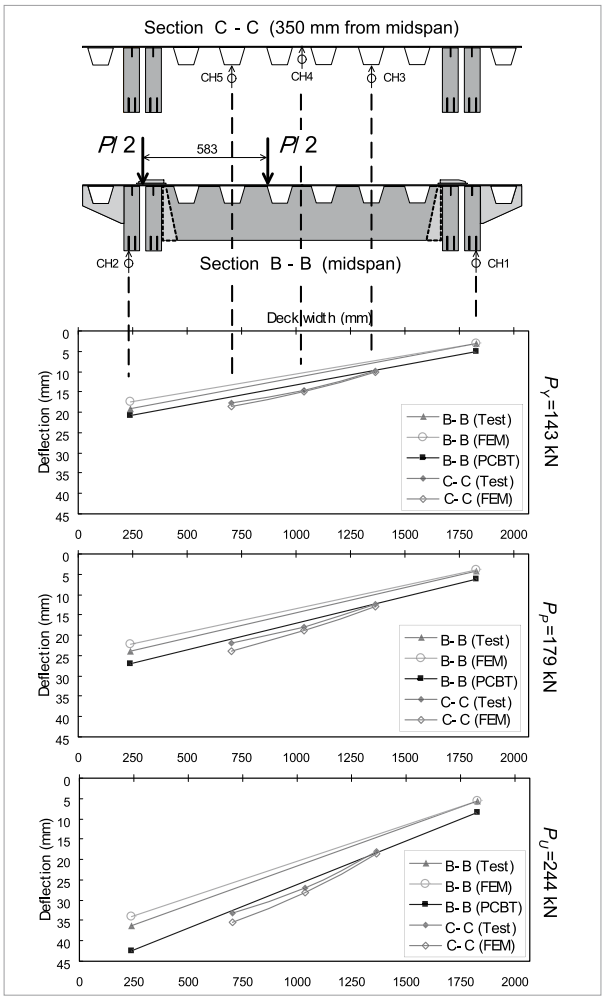

Fig. 12 Deflection distribution at applied loads P_N (N = Y, P, U)

12. ábra A behajlás eloszlása az alkalmazott P_N terheléseknél

deflection meters CH3, CH4 and CH5 are shown. Then, deflection values calculated by FEM analysis are included for the same sections. Finally, for glulam main beams at section B-B, deflection values determined analytically by the plastic composite beam theory (PCBT) are also included.

Comparing these three sets of values to each other, a good agreement can be observed, calculated values from the FEM analysis closely following the measured data. Compared to measured deflections, deflections obtained from FEM are larger for the U-ribs and smaller for the main beams, due to a simplified approach in the analysis, regarding the connection between the structural members. All deflection values that were used to construct Fig. 12 are shown in a tabulated form in Table 2. In addition to the deflection data at applied truck wheel loads P_N (N = Y, P, U), measured deflections and deflections calculated by the FEM analysis are also included for the experimental ultimate load $P_{U,exp,}$ to demonstrate the good agreement between the two sets of data. For section C-C, deflections calculated by the plastic composite beam theory are not available.

Fig. 13 shows a lateral view of the longitudinal strain distribution of glulam main beams at the ultimate load P_U = 244 kN, determined by the plastic composite beam theory. Measured and calculated strain values are included, FEM strain distribution following closely the measured one. For G4 and G3, measured strain values and strains determined by the FEM analysis are also included for the deck plate and lower rib at each section considered. Composite action could not be achieved completely between deck plate, glulam beam and lower ribs, therefore differences appeared between the strain values of these members.

Table 2 Measured and calculated deflections at applied loads P_N (N = Y, P, U) for load case LC2

2. táblázat Mért és számított behajlások az alkalmazott P_N terheléseknél (N = Y, P, U) az LC2 terhelés esetében

Section	Defl. meter	P_Y = 143 kN			P_P = 179 kN			P_U = 244 kN			$P_{U,exp}$ = 266 kN	
		∂ (mm)			∂ (mm)			∂ (mm)			∂ (mm)	
		Test	FEM	PCBT	Test	FEM	PCBT	Test	FEM	PCBT	Test	FEM
B-B	CH2	19,3	17,3	20,7	23,9	22,2	27,0	36,3	31,1	42,4	44,6	40,0
	CH1	3,2	3,1	5,0	4,1	4,0	6,3	5,7	5,6	8,5	6,2	6,1
C-C	CH5	17,8	18,6	N/A	21,9	23,8	N/A	33,1	35,5	N/A	40,0	40,9
	CH4	14,6	14,8	N/A	18,1	18,9	N/A	26,9	28,0	N/A	32,1	32,0
	CH3	9,9	10,0	N/A	12,3	12,8	N/A	17,9	18,5	N/A	20,9	21,0

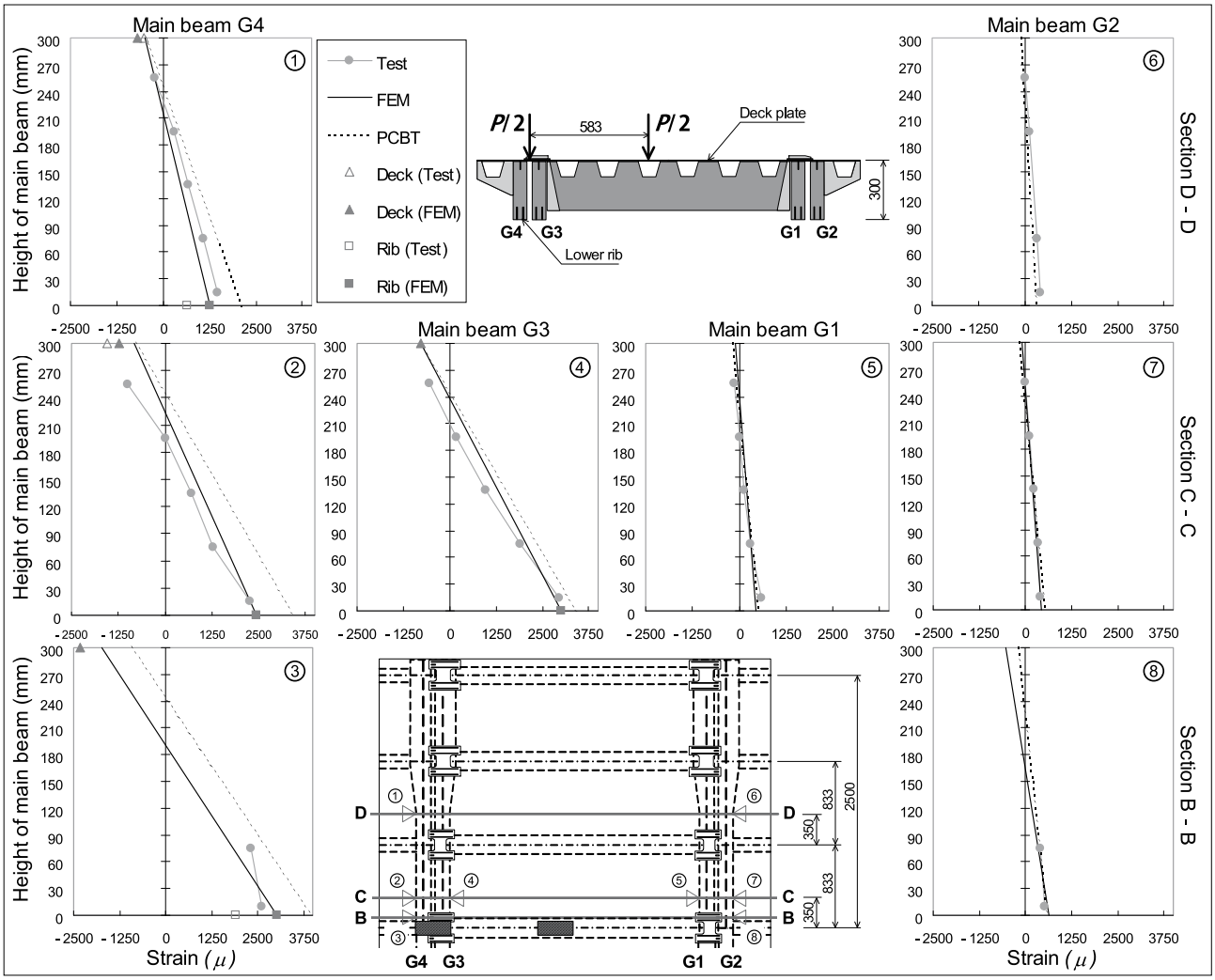

Fig. 13 Longitudinal strain distribution of glulam main beams at ultimate load P_U = 244 kN (lateral view)

13. ábra A rétegelt-ragasztott főtartók longitudinális igénybevétel-eloszlása P_U=244kN nagyságú végterhelésnél (oldalnézet)

Conclusions

A non-linear three-dimensional FEM analysis was performed in order to compare the performance and calculated results with measured data of a one-third-scale timber-steel hybrid bridge model. Test and FEM results showed a good agreement for the strain distribution of glulam main beams. However, when comparing deflection data, timber main beams were stiffer in the FEM analysis and steel deck was stiffer in the test. The reason was the absence of connection details between structural members in the FEM model at this stage. Also, glue line represented a major cause of premature failure in the failure test. Since glue properties seem critical for this system, in the future they need to be included in the FEM model, together with refined connection details.

Besides the above, a new timber-steel hybrid system was developed. The new structure keeps the timber main beams, but replaces the steel deck-timber floor beam configuration with longitudinal steel square tubes, connected to each other at certain intervals through transverse steel pipes embedded in concrete. The authors intend to present the structural performance of this new timber-steel hybrid system in a future paper.

References

Kiss L, Sasaki T, Iijima Y, Usuki S (2008) Failure test and finite element analysis of timber-steel hybrid bridge, Proceedings of the 10th World Conference on Timber Engineering, 3-107p.pdf

Kiss L, Sasaki T, Iijima Y, Usuki S (2007a) FEM analysis of timber-steel hybrid bridge structure, JSCE Proceedings of the 6th Symposium on Timber Bridges, pp. 27-34

Kiss L, Sasaki T, Usuki S (2007b) Finite element modeling of timber-steel hybrid bridge, Proceedings of the 62nd Annual Conference of the Japan Society of Civil Engineers, pp. 297-298

Kiss L, Sasaki T, Toyota A, Usuki S (2006a) Performance of glulam beam-orthotropic steel deck hybrid bridge structure, Proceedings of the 9th World Conference on Timber Engineering, 2.10.4.pdf

Kiss L, Sasaki T, Usuki S (2006b) Behavior of glulam beam-orthotropic steel deck hybrid bridge structure, JSCE Proceedings of the 5th Symposium on Timber Bridges, pp. 101-106

Miki C, Suganuma H, Tomizawa M, Machida F (2005) Cause study on fatigue damage in orthotropic steel bridge deck, Proceedings of the Japan Society of Civil Engineers, No. 780, I-70, pp. 57-69 (in Japanese)

Pousette A (2003) Full-scale test and finite element analysis of a wooden spiral staircase, Holz Roh-Werkst. 61:1-7

Dunántúli tölgyek gesztesedési folyamatai

FEHÉR Sándor[1], KRAJCSÁK Zoltán[2]

[1] NymE, Faanyagtudományi Intézet

[2] Budapesti Műszaki és Gazdaságtudományi Egyetem, Menedzsment és Vállalatgazdaságtan Tanszék

Kivonat

A fatest két, különböző tulajdonságokkal rendelkező részre, a szíjácsra és a gesztre bontható. A faipari hasznosítás szempontjából az utóbbinak van kiemelkedő jelentősége, amit elsősorban e fa-rész nagyobb tartóssága és jobb műszaki tulajdonságai eredményeznek. A színes gesztű fajoknál a feldolgozás során igyekszünk is ezt figyelembe venni a szíjács kiejtésével. Különösen igaz ez a tölgyekre. A jellemzően állományalkotó, fényigényes tölgy az egyik legértékesebb lombos fafajunk, feldolgozása rendkívül széleskörű területeket érint. Hazai erdeink fatömegének több mint harmadát a tölgy fajok teszik ki. A tölgyek gesztesedési folyamatát – csakúgy, mint bármely más fafajét – nagyon sok tényező határozza meg. A legfontosabb talán az adott fa genetikai jellemzői, azaz a fafaj határozza meg a gesztesedés jellegzetességeit. Azonban számos külső tényező is meghatározó jelentőséggel rendelkezik, mint a növekedés körülményei (alászorultság, záródás, stb.) és az ökológiai jellemzők (földrajzi elhelyezkedés, klíma, termőhely, hidrológia, stb.). A gesztesedés körülményeinek hatását sajnos már nem értékelik, annak ellenére, hogy azok jelentősége igen nagy. Új megközelítést adhat a tölgy állományok minőségi javítása szempontjából a kitermelt faanyag geszt-szíjács arányának vizsgálata. A geszt arányának növekedése számos előny közül elsősorban gazdasági előnyöket eredményez, így a gesztesedés mértékének